

High-Performance Single-Crystalline Perovskite Thin-Film Photodetector

Zhenqian Yang, Yuhao Deng, Xiaowei Zhang, Suo Wang, Huazhou Chen, Sui Yang, Jacob Khurgin, Nicholas X. Fang, Xiang Zhang, and Renmin Ma*

The best performing modern optoelectronic devices rely on single-crystalline thin-film (SC-TF) semiconductors grown epitaxially. The emerging halide perovskites, which can be synthesized via low-cost solution-based methods, have achieved substantial success in various optoelectronic devices including solar cells, lasers, light-emitting diodes, and photodetectors. However, to date, the performance of these perovskite devices based on polycrystalline thin-film active layers lags behind the epitaxially grown semiconductor devices. Here, a photodetector based on SC-TF perovskite active layer is reported with a record performance of a 50 million gain, 70 GHz gain-bandwidth product, and a 100-photon level detection limit at 180 Hz modulation bandwidth, which as far as we know are the highest values among all the reported perovskite photodetectors. The superior performance of the device originates from replacing polycrystalline thin film by a thickness-optimized SC-TF with much higher mobility and longer recombination time. The results indicate that high-performance perovskite devices based on SC-TF may become competitive in modern optoelectronics.

Single-crystalline thin-film (SC-TF) materials are the cornerstone of modern electronic and photonic devices due to their distinct properties including low trap density, high mobility, and well-defined thickness. Nowadays, epitaxial growth technology^[1,2] can control the thickness of SC-TF down to monolayer level with high material purity. However, epitaxial growth requires lattice constant and expansion coefficient matches with substrates as well as high vacuum and temperature growth conditions.^[1,2]

Z. Yang, Y. Deng, Dr. X. Zhang, S. Wang, H. Chen, Prof. R. Ma
State Key Lab for Mesoscopic Physics and School of Physics
Peking University
Beijing 100871, China
E-mail: renminma@pku.edu.cn

Dr. S. Yang, Prof. X. Zhang
Department of Mechanical Engineering
University of California
Berkeley, CA 94720, USA

Prof. J. Khurgin
Department of Electrical and Computer Engineering
Johns Hopkins University
Baltimore, MD 21218, USA

Prof. N. X. Fang
Department of Mechanical Engineering
Massachusetts Institute of Technology
Cambridge, MA 02139, USA

DOI: 10.1002/adma.201704333

Recently, halide perovskites that can be grown by low-cost solution-based methods have emerged as a new class of semiconductor for high-performance optoelectronic devices, such as solar cells,^[3–5] light-emitting diodes and lasers,^[6–8] laser cooling,^[9,10] and photodetectors.^[11] For instance, the photovoltaic efficiency of halide-perovskite-based solar cells has reached over 20% in a few years, approaching that of single-crystalline silicon cells.^[12] This progress has been largely achieved by improving the crystalline quality.^[13–22] This effort of quality improvement has also led to the reported progress in perovskite thin-film photodetectors.^[23–33]

In 2015, inverse temperature crystallization method has been developed to grow macroscale single-crystalline halide perovskites.^[34–36] As expected, these macroscale single crystals show superior

physical properties than their polycrystalline counterpart.^[37–56] Their mobility can be over $100 \text{ cm}^2 \text{ V}^{-1} \text{ s}^{-1}$ and trap density can be as low as 10^9 cm^{-3} , both of which are orders of magnitude better than polycrystalline thin films.^[33–40] Although with a much thicker thickness than the polycrystalline thin film, these bulk crystals find unique applications with high performances and stability in narrowband photon detection and X-ray detection, etc.^[35,57–60]

To improve the suitability of perovskites in most optoelectronic devices, including solar cells, photodetectors, light-emitting diodes, lasers, etc., achieving simultaneously good crystallinity and proper thickness is essential. However, the aspect ratios of these macroscale single crystals have been limited to about unity depending on the isotropous growth rate in solution. Most recently, spatially limited condition has been introduced to grow perovskite crystals with improved aspect ratio.^[61–65] Compared to the bulk crystals, these perovskite crystals with reduced thickness show significantly improved performance in solar cells as well as in photodetectors.^[61–64]

However, to date, single-crystalline perovskite-based devices including solar cells and photodetectors all have the active layers thicker than several micrometers. Due to its high absorption coefficient, perovskite materials can absorb the incident light completely in hundreds of nanometers. Compared to the optimized film thickness in this range in devices based on polycrystalline films, the unnecessarily thick active layer in single-crystalline perovskite-based devices leads to a longer transit

time and a larger recombination probability for the photon-excited carriers, which degrades the device performance. Notwithstanding the growing body of work on perovskite devices, it is still very challenging to achieve simultaneously good crystallinity and proper thickness of perovskites in optoelectronic devices.

Here, we report a photodetector based on SC-TF perovskite active layer with an optimized thickness down to hundreds of nanometers. The device achieves a record photoconductive gain of 50 million and a gain-bandwidth product of 70 GHz. The superior performance of our SC-TF perovskite photodetectors has also been confirmed by their ultrahigh sensitivity with record detection limit down to 100-photon level at 180 Hz modulation bandwidth, which is over 50 times lower than all previously reported perovskite photodetectors. The dynamic range and specific detectivity of the SC-TF perovskite photodetector are about 83 dB and $1.3 \times 10^{13} \text{ cm Hz}^{0.5} \text{ W}^{-1}$, respectively. The superior performance of our devices originates from replacing polycrystalline thin film with the thickness optimized SC-TF. To further illustrate the crucial role of SC-TF thickness, we have systematically investigated the thickness-dependent performance of SC-TF perovskite photodetectors. With the SC-TF thickness decreasing from about 10 μm to hundreds of nanometers, the lowest detectable power and internal gain improve two and four orders of magnitude, respectively.

The intrinsic merit of perovskite for photon detection is its high absorption coefficient and internal quantum efficiency. Photoconductive gain (G) can be expressed as $G = \frac{\tau}{\tau_{tr}} \eta$, where τ is the lifetime of trapped carriers, τ_{tr} is the carrier transit time, and η is the external quantum efficiency of the device. τ_{tr} , assuming uniform field and no velocity saturation, roughly equals $\frac{d^2}{\mu V}$, where d and μ are the thickness and mobility of

the active layer, respectively, and V is the applied voltage.^[66,67] η equals $(1 - \mathfrak{R})\xi(1 - e^{-\alpha d})$, where \mathfrak{R} is the reflection ratio of the incident light, ξ is internal quantum efficiency, and α is absorption coefficient of the active material.^[66,67] From a point of view of device performance, higher α and ξ of the active layer indicate a more efficient photon-to-carrier conversion power. With an optimized thickness, devices based on polycrystalline perovskite show a remarkable performance. A further performance improvement is however constrained by their limited mobility. For instance, the mobility of MAPbBr₃ polycrystalline film is only about $0.26 \text{ cm}^2 \text{ V}^{-1} \text{ s}^{-1}$, which is over 200 times lower than its single-crystalline counterpart.^[33] In contrast to the reported perovskite devices based on polycrystalline or too thick single-crystalline active layer, here we exploit an SC-TF perovskite active layer with an optimized thickness for photon detection.

Figure 1a shows the optical image of an MAPbBr₃ SC-TF (MA = CH₃NH₃⁺) with a thickness of about 365 nm and a side length >600 μm , corresponding to an aspect ratio >1500 (Section S1, Supporting Information). Figure 1b shows a scanning electron microscope (SEM) image of an MAPbBr₃ SC-TF, indicating it with a smooth surface and free from grain boundaries. Quantitative surface analysis is conducted by atomic force microscope surface scan, which shows a low surface roughness with a root mean square (RMS) of $\approx 0.54 \text{ nm}$ within a $25 \mu\text{m}^2$ area (Section S2, Supporting Information). We fabricate the MAPbBr₃ SC-TF photodetector based on an MAPbBr₃/Au Schottky diode. MAPbBr₃ SC-TF was first grown on the ITO substrate. Following that a hard mask had been put on the top surface of the film. A circular Au electrode (100 μm in diameter and 50 nm in thick) was then thermally deposited on the top surface of the film in the vacuum chamber. Figure 1c shows the cross-profile SEM image of a typical device, where the thickness of the MAPbBr₃ SC-TF

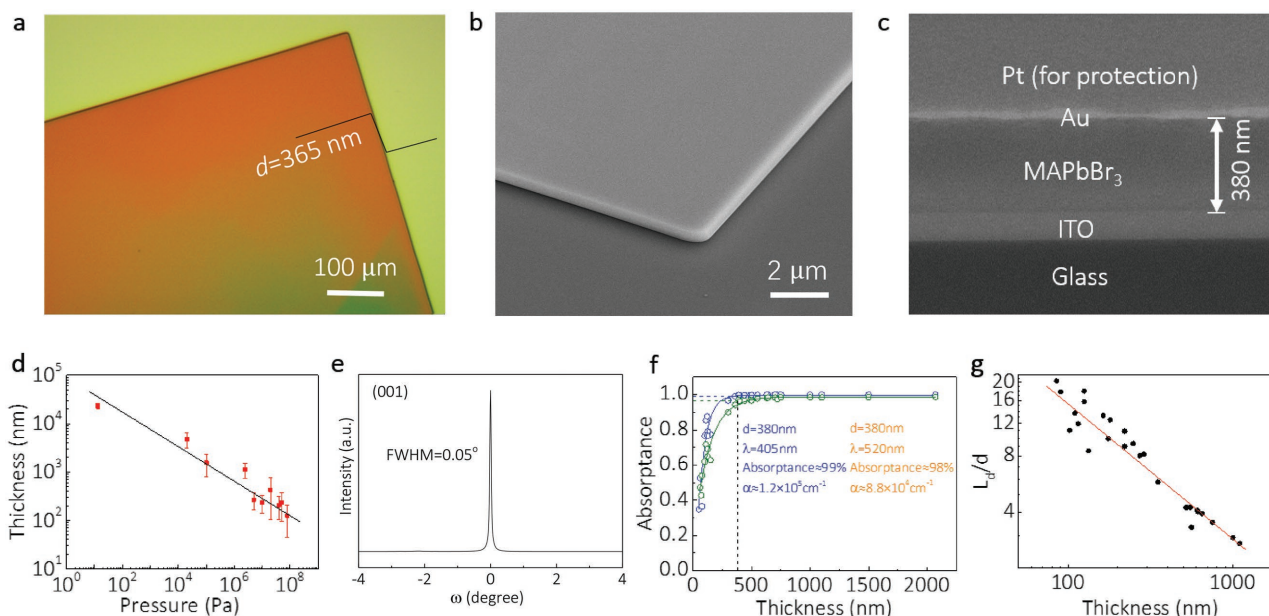


Figure 1. Morphology and property of the single-crystalline perovskite thin film. a) The optical image of a single-crystalline perovskite thin film with a thickness of 365 nm. b) SEM image of a single-crystalline perovskite thin film. c) The cross-profile SEM image of a photodetector based on single-crystalline perovskite thin film. d) Thickness of the film under different pressure growth conditions. e) Rocking wave data of the (001) peak. f) Absorbance of the film with different thicknesses. g) Ratio of diffusion length over film thickness versus film thickness.

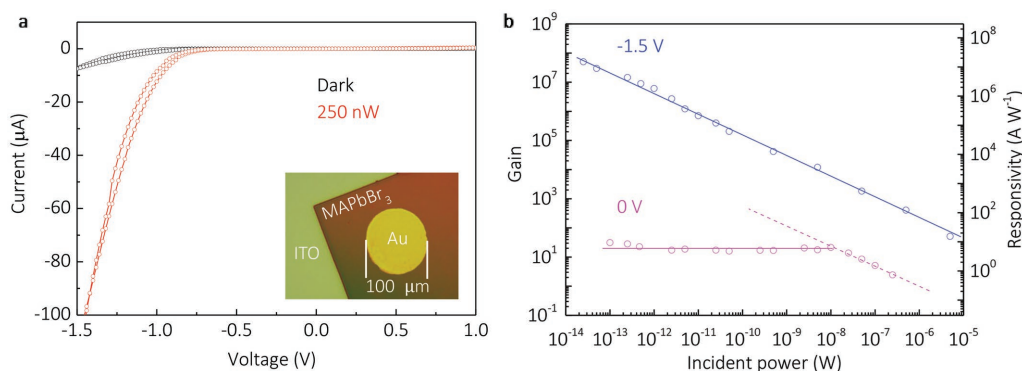


Figure 2. Photoreponse, gain, and responsivity of the photodetector. a) I - V curves in forward and backward sweeping directions of a photodetector under dark and 250 nW illumination conditions. Under both conditions, I - V curves clearly show rectifying behavior. And the diode is open when negative bias is applied, which indicates that the Schottky barrier forms at MAPbBr₃/Au interface. Inset: Optical image of the device. b) Gain and responsivity of the device. The highest gain and responsivity are about 5×10^7 and 1.6×10^7 A W⁻¹, respectively.

active layer is 380 nm. The uniform phase of SC-TF layer free from grain boundaries shows the great crystallinity of the film.

For the growth of such an SC-TF, we introduce three improvements to the previously reported inverse temperature crystallization technique. First, the crystal is grown inside two face-to-face substrates with a micrometer-sized gap to break isotropic growth condition (Section S3, Supporting Information).^[62–65] Second, the thickness is controlled by the pressure applied on the gap.^[65] Figure 1d shows that the thickness of the film decreases linearly with pressure under logarithmic coordinates over three orders and reaches to 100 nm level under 10^8 Pa. Third, we control the nucleation process to limit the number of crystal seeds formed inside the gap by substrate surface modifications (Section S3, Supporting Information). X-ray diffraction and transmission X-ray microscopy results confirm that the whole thin film is with a single-crystalline structure and the crystal orientation in vertical direction is (001) (Section S4, Supporting Information). The full width at half-maximum of the (001) peak from the rocking curve is 0.05° as shown in Figure 1e. As a qualitative indication of crystallinity, this value is consistent with that of the reported bulk MAPbBr₃ crystals.^[68] We measure the trap density and mobility to characterize the electrical properties of the MAPbBr₃ SC-TF by space-charge-limited current analysis (Section S5, Supporting Information) and Hall effect (Section S6, Supporting Information), respectively. The measured trap density is 1.6×10^{11} cm⁻³ and the mobility is about 60 cm² V⁻¹ s⁻¹, both of which are orders of magnitude better than MAPbBr₃ polycrystalline films fabricated by spin-coating methods and comparable to the large single crystal.^[33–40] We also measured the lifetime of the carriers in the film with different thicknesses (Section S7, Supporting Information). The lifetime of the bulk single crystal is 242 ns, consistent with the value reported by others.^[34]

The thickness of the SC-TF is optimized to ≈ 380 nm for a higher carrier collection efficiency and nearly 100% absorption of the incident light. Figure 1f shows the relationships between the absorptance ($A = \frac{P_a}{P_i}$, where P_a is the light power absorbed by the film and P_i is the incident light power) and the film thickness at 520 and 405 nm. The two curves show a similar trend where the absorptance reaches over 98% at a film thickness of ≈ 380 nm. The absorption coefficient (α) can be

calculated from these curves. For incident wavelengths at 520 nm and 405 nm, absorption coefficients are 8.8×10^4 cm⁻¹ and 1.2×10^5 cm⁻¹, respectively (Section S8, Supporting Information). The carrier diffusion length of the SC-TF is about a few micrometers, which is much longer than the SC-TF thickness (Section S7, Supporting Information). Figure 1g shows the ratio of the diffusion length (L_d) over the SC-TF thickness (d) versus film thickness, characterizing the feasibility of the photon-excited carrier collection. We can see that the L_d/d decreases with the thickness of the thin film, indicating that the carriers in thinner film will be collected more easily. The vertical structure based on thickness-optimized SC-TF layer simultaneously ensures high absorption, short transit distance, and therefore short transit time of carriers, leading to a more efficient photon-to-carrier conversion and low recombination probability of photogenerated carriers and hence to a superior performance of photodetector.

Figure 2a, inset, shows the top view of the device. In the electrical characterization, the ITO substrate is grounded. In the photo-detecting characterization, a 405 nm laser spot with a diameter of about $500 \mu\text{m}$ was used to illuminate the device (Section S9, Supporting Information). Figure 2a shows the I - V curves of the device under dark condition and an illumination condition of 250 nW. Under both conditions, I - V curves clearly show rectifying behavior. The diode is open when negative bias is applied, indicating that a Schottky barrier is formed at MAPbBr₃/Au interface. At the negative bias of -1.5 V, the current increases over one order of magnitude due to the incident light. The pronounced response originates from two separate effects. First, the carrier density increases in the MAPbBr₃ SC-TF under optical illumination. Second, the height of Schottky barrier gets reduced due to the trapped photon-excited electrons at the MAPbBr₃/Au interface.^[69–71]

In order to quantitatively study the response of our device, we measured gain of the device. As mentioned above, photoconductive gain originates from the difference between the carrier lifetime and transit time. The lifetime of trapped electrons is much longer than the transit time of free holes. When the photon-excited electrons are trapped, the number of holes injected in the active layers and then passed through the circuit before recombining with electrons greatly exceeds the number of the originally generated carriers. The resulting photoconductive gain can be calculated by $\frac{(J_{\text{light}} - J_{\text{dark}})/e}{P/h\nu}$,

where e is electronic charge and $h\nu$ is the incident photon energy.^[66,67]

Figure 2b shows illumination power dependence of the gain in our device at -1.5 and 0 V. When there is an external bias of -1.5 V, gain continuously increases with the decrease of the incident power and reaches the maximum of 5.0×10^7 at an incident power of 25 fW. The corresponding responsivity $R = \frac{G}{h\nu/e}$ is also shown in the figure. The largest responsivity of the device is 1.6×10^7 A W⁻¹. The trend of the illumination-power-dependent gain comes from the large amount of the external bias injected electrons, which saturate all the trap states at the MAPbBr₃/Au interface.^[71–74] When the incident power decreases, the ratio of the trapped electrons increases, leading to an increase in the gain. As far as we know, both of the gain and responsivity of our device are over 5000 times higher than all the reported perovskite photodetectors.

At 0 V bias, the device can operate in a photovoltaic rather than photoconductive regime. In contrast with the gain behavior at -1.5 V, we observe a distinct kink at 10 nW. Below 10 nW, the value of gain maintains a constant at about 10. The low incident power leads to a small number of photon-excited electrons, which will be all trapped by trap states. The same mechanism of amplification for all the photon-excited carriers leads to a constant gain. Above 10 nW, photon-excited carriers start to saturate all the trap states and thus the gain decreases with the increase of the incident power, showing the same trend as in the case of -1.5 V. However, the gain at 0 V is smaller than that at -1.5 V at the same incident power because

carriers' transit time through the device is much shorter at -1.5 V.

Specific detectivity characterizes the ability of photodetector to detect weak signals in the presence of shot and generation-recombination noise and can be calculated by $\frac{R\sqrt{A}}{\sqrt{2GeI_d}}$, where I_d is the dark current and A is the area of the device.^[66,67] At -1.5 V bias and 25 fW illumination, the corresponding specific detectivity is 1.3×10^{13} cm Hz^{0.5} W⁻¹. Such a large responsivity of the device weakens the restriction of shot noise from dark current (Section S10, Supporting Information), and the value we obtained is close to these perovskite photodetectors with the highest specific detectivity.^[11] The values of specific detectivity and gain remain almost the same spanning the measured wavelength from 405 to 505 nm (Section S10, Supporting Information).

The linear dynamic range (LDR) can be calculated by $10 \log \frac{P_{\max}}{P_{\min}}$, where P_{\max} and P_{\min} are the maximum and minimum values of incident power in the photocurrent linear range, respectively. LDR is shown in Figure 3a by the variation of photocurrent with the incident power at -1.5 V and 0 V bias. At -1.5 V, the photocurrent increases linearly in all the measurement range (from 25 fW to 5 μ W) in logarithmic coordinates, indicating that LDR is 83 dB. We note that such a value is limited by the output power of our 405 nm laser, and LDR might further increase if higher incident power is applied. At 0 V, a kink appears at 10 nW. Below 10 nW, the trap states are unsaturated and the photocurrent increases linearly with the incident power, indicating an LDR of 50 dB. Above 10 nW, all

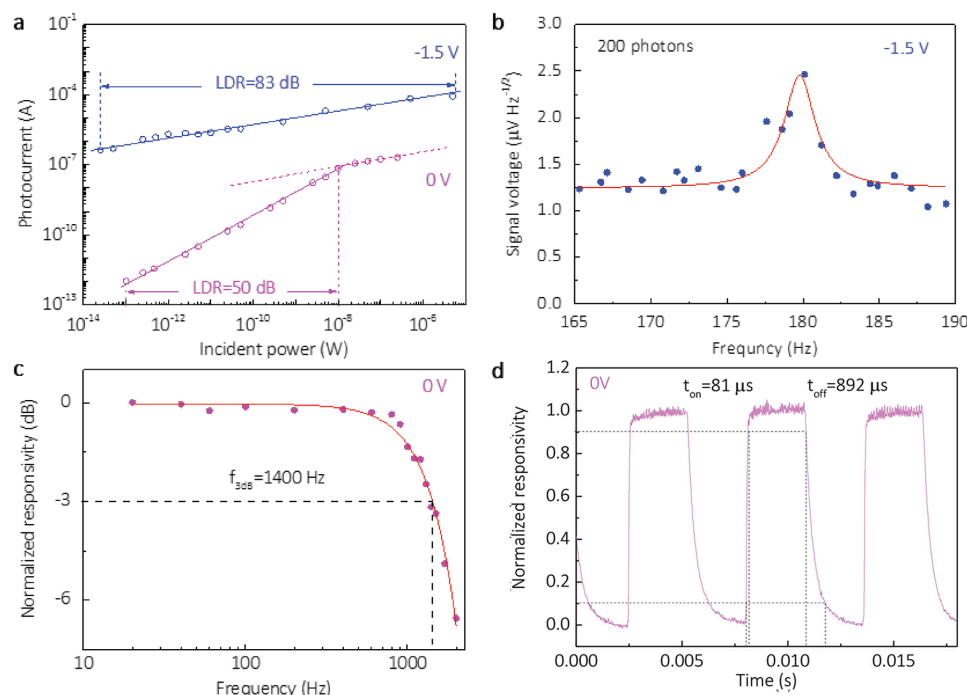


Figure 3. Linear dynamic range, detection limit, and the 3dB bandwidth of the photodetector. a) Photocurrent versus incident power. The linear dynamic range of the detector is 83 dB at -1.5 V bias and 50 dB at 0 V bias. b) Lowest number of photons that the device can response. The device can response to 200 photons in each pulse of the incident light at 180 Hz at -1.5 V bias. c) 3 dB bandwidth of the device at 0 V bias. d) Time domain response of the self-powered current.

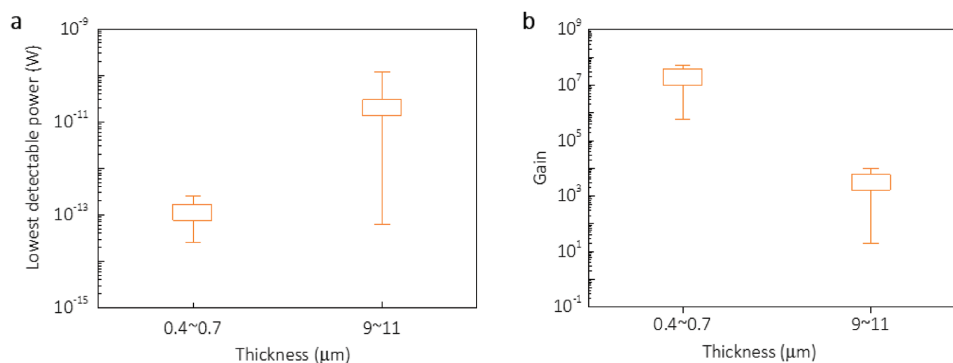


Figure 4. Perovskite thickness-dependent performance. We measured five devices with thicknesses in the range of 400–700 nm, and as a comparison, another six devices with thicknesses in the range of 9–11 μm. a) Averaged minimum detectable power of these devices in the two thickness ranges. b) Averaged maximum gain of these devices in the two thickness ranges. The thinner devices have much better performance than the thicker devices in both characterized parameters.

the trap states are saturated by photon-excited carriers and lead to a lower amplification of current. To evaluate the capability of the device for weak light detection, we measured the minimum number of photons to which the device can respond. In the photodetecting characterization, the 405 nm illumination laser is modulated at 180 Hz by an optical chopper. In the electrical characterization, the applied external voltage is -1.5 V, and a 2 MΩ resistance is connected in series with the detector to extract the signal. A lock-in amplifier is used to detect the signal voltage. Reference wave with frequency from 165 to 190 Hz is generated by a signal generator. The signal spectrum is shown in Figure 3b. The peak at 180 Hz indicates that the device does have a response to the modulated illumination. The base line represents the background noise. As the incident power decreases, the signal becomes smaller (Section S11, Supporting Information). When the signal-to-noise ratio is 1 (Figure 3b), the corresponding incident power is 35 fW which represents the detection limit or noise equipment power of the device.^[66] At the detection limit, the number of photons in each pulse is only about 200. (Section S11, Supporting Information) Such a detection limit is over 50 times lower than all reported perovskite photodetectors.^[26,27] The high performance of the SC-TF perovskite photodetector for weak light detection mainly benefits from two factors. First, the optimized thickness of MAPbBr₃ SC-TF leads to a nearly 100% absorption of the incident photons while keeping the carriers transit distance as short as possible. Second, the high crystallinity of the SC-TF and the short transit distance reduce the recombination loss of photon-excited carriers.

We noted that when the device is kept biased at -1.5 V, there is a gradual reduction process in the response of the detector due to ions migration (Section S12, Supporting Information). When perovskite is under an external bias and the applied energy is over the ions' activation energy, ions would migrate to the adjacent intrinsic vacancy defect. This phenomenon is pervasive in perovskite.^[75] However, it can be mitigated at a lower external bias.^[76] To characterize the stability of our photodetectors, we measured the self-powered photocurrent of a device before and after 8 d of storage. The device shows stable performance in each continuously illuminated 7 h and over days (Section S13, Supporting

Information). The measured detection limit is about 600 photons at 0 V. And the 3 dB bandwidth is 1400 Hz as shown in Figure 3c. Figure 3d shows the time domain response of the self-powered current of a device. The rise and fall times are about 81 and about 890 μs, respectively (Section S14, Supporting Information). The gain-bandwidth product of our device is 70 GHz, which is, to our knowledge, two orders of magnitude higher than all the perovskite detectors based on the photoconducting mechanism (Section S15, Supporting Information).^[11,77,78]

Finally, we systematically study the thickness-dependent performance of SC-TF perovskite photodetectors. Here, the thickness of the MAPbBr₃ SC-TF active layer determines the carrier transit distance, which is one of the key parameters to influence the performance of the detector. We measured five devices with thicknesses in the range of 400–700 nm, and as a comparison, another six devices with thicknesses in the range of 9–11 μm. All of them are measured at -1.5 V bias. **Figure 4a** shows the averaged minimum detectable power by each of these devices in the two thickness ranges. **Figure 4b** shows the averaged maximum gain that can be achieved by each of these devices in the two thickness ranges. As we can see, the thinner devices have much better performance than the thicker devices in both parameters. With the SC-TF thickness decreasing from about 10 μm to hundreds of nanometers, the minimum detectable power and internal gain improve two and four orders of magnitude, respectively. Providing a sufficient absorption, a thinner SC-TF reduces the recombination probability and enlarges the collection efficiency of the carriers, which are crucial for weak signal detection. For the gain, a thinner SC-TF leads to a shorter transit time of the carriers and consequently a higher gain. To further improve the performance of the detector, an antireflective layer is necessary to reduce the reflection of the incident light. The thickness of the active layer can be further optimized to the best state to compromise the tradeoff between the light absorption and the carrier collection. For the applications where only specific wavelength should be detected, a coherence absorption condition can be engineered to enhance the absorption of the active layer at thickness even at tens of nanometers, and consequently much higher carrier collection efficiency can be achieved.^[79]

In summary, we report that a photodetector based on perovskite SC-TF can have superior performance than its polycrystalline counterpart. By simultaneously optimizing the perovskites thickness and crystallinity, the device achieves a record photoconductive gain of 50 million and a gain-bandwidth product of 70 GHz. The superior performance of SC-TF perovskite photodetectors has also been exemplified by their ultrahigh sensitivity with record detection limit down to 100-photon level. Further, we systematically study the thickness-dependent performance of photodetectors. We find that a suitable thickness of the perovskite SC-TF is crucial in device performance. With the SC-TF thickness decreasing from about 10 μm to hundreds of nanometers, the lowest detectable power and internal gain improve two and four orders of magnitude, respectively. Our results show that perovskite devices based on SC-TF have a bright future for optoelectronics.

Supporting Information

Supporting Information is available from the Wiley Online Library or from the author.

Acknowledgements

Z.Y., Y.D., and Dr. X.Z. contributed equally to this work. This work was supported by the National Natural Science Foundation of China (Grant Nos. 11574012, 11774014, and 61521004) and the "Youth 1000 Talent Plan." The research is partially supported by Office of Naval Research (ONR) Multidisciplinary University Research Initiative (MURI) program under Grant No. N00014-17-1-2588 and the King Abdullah University of Science and Technology Office of Sponsored Research (OSR) (Award OSR-2016-CRG5-2950-03).

Conflict of Interest

The authors declare no conflict of interest.

Keywords

gain, halide perovskite, photodetectors, single-crystalline thin films

Received: August 1, 2017
Revised: October 30, 2017
Published online: January 8, 2018

- [1] A. G. Thompson, *Mater. Lett.* **1997**, *30*, 255.
- [2] M. A. Herman, H. Sitter, *Molecular Beam Epitaxy: Fundamentals and Current Status*, Springer-Verlag, New York **2012**.
- [3] M. A. Green, A. Ho-Baillie, H. J. Snaith, *Nat. Photonics* **2014**, *8*, 506.
- [4] C. Zuo, H. J. Bolink, H. Han, J. Huang, D. Cahen, L. Ding, *Adv. Sci.* **2016**, *3*, 7.
- [5] J. P. Correabaena, A. Abate, M. Saliba, W. Tress, T. J. Jacobsson, M. Grätzel, A. Hagfeldt, *Energy Environ. Sci.* **2017**, *10*, 710.
- [6] S. D. Stranks, H. J. Snaith, *Nat. Nanotechnol.* **2015**, *10*, 391.
- [7] B. R. Sutherland, E. H. Sargent, *Nat. Photonics* **2016**, *10*, 295.
- [8] S. A. Veldhuis, P. P. Boix, N. Yantara, M. Li, T. C. Sum, N. Mathews, S. G. Mhaisalkar, *Adv. Mater.* **2016**, *28*, 6804.
- [9] J. Zhang, Q. Zhang, X. Wang, L. C. Kwek, Q. Xiong, *Nat. Photonics* **2016**, *10*, 600.
- [10] S. T. Ha, C. Shen, J. Zhang, Q. Xiong, *Nat. Photonics* **2016**, *10*, 115.
- [11] F. P. G. D. Arquer, A. Armin, P. Meredith, E. H. Sargent, *Nat. Rev. Mater.* **2017**, *2*, 16100.
- [12] Best Research-Cell Efficiencies, <https://www.nrel.gov/pv/assets/images/efficiency-chart.png>, National Renewable Energy Laboratory (accessed: July 2017).
- [13] A. Kojima, K. Teshima, Y. Shirai, T. Miyasaka, *J. Am. Chem. Soc.* **2009**, *131*, 6050.
- [14] H. S. Kim, C. R. Lee, J. H. Im, K. B. Lee, T. Moehl, A. Marchioro, S. J. Moon, R. Humphry-Baker, J. H. Yum, J. E. Moser, M. N. Grätzel, G. Park, *Sci. Rep.* **2012**, *2*, 591.
- [15] M. M. Lee, J. Teuscher, T. Miyasaka, T. N. Murakami, H. J. Snaith, *Science* **2012**, *338*, 643.
- [16] N. J. Jeon, J. H. Noh, Y. C. Kim, W. S. Yang, S. Ryu, S. I. Seok, *Nat. Mater.* **2014**, *13*, 897.
- [17] W. S. Yang, J. H. Noh, N. J. Jeon, Y. C. Kim, S. Ryu, J. Seo, S. I. Seok, *Science* **2015**, *348*, 1234.
- [18] C. Bi, Q. Wang, Y. Shao, Y. Yuan, Z. Xiao, J. Huang, *Nat. Commun.* **2015**, *6*, 7747.
- [19] W. Nie, H. Tsai, R. Asadpour, J. C. Blancon, A. J. Neukirch, G. Gupta, J. J. Crochet, M. Chhowalla, S. Tretiak, M. A. Alam, H. L. Wang, A. D. Mohite, *Science* **2015**, *347*, 522.
- [20] N. Ahn, D. Y. Son, I. H. Jang, S. M. Kang, M. N. Choi, G. Park, *J. Am. Chem. Soc.* **2015**, *137*, 8696.
- [21] D. Bi, C. Yi, J. Luo, J. D. Décoppet, F. Zhang, S. M. Zakeeruddin, X. Li, A. Hagfeldt, M. Grätzel, *Nat. Energy* **2016**, *1*, 16142.
- [22] X. Li, D. Bi, C. Yi, J. D. Décoppet, J. Luo, S. M. Zakeeruddin, A. Hagfeldt, M. Grätzel, *Science* **2016**, *353*, 58.
- [23] H. R. Xia, J. Li, W. T. Sun, L. M. Peng, *Chem. Commun.* **2014**, *50*, 13695.
- [24] Q. Lin, A. Armin, D. M. Lyons, P. L. Burn, P. Meredith, *Adv. Mater.* **2015**, *27*, 2060.
- [25] D. Li, G. Dong, W. Li, L. Wang, *Sci. Rep.* **2015**, *5*, 7902.
- [26] R. Dong, Y. Fang, J. Chae, J. Dai, Z. Xiao, Q. Dong, Y. Yuan, A. Centrone, X. C. Zeng, J. Huang, *Adv. Mater.* **2015**, *27*, 1912.
- [27] Y. Fang, J. Huang, *Adv. Mater.* **2015**, *27*, 2804.
- [28] W. Hu, W. Huang, S. Yang, X. Wang, Z. Jiang, X. Zhu, H. Zhou, H. Liu, Q. Zhang, X. Zhuang, J. Yang, D. H. Kim, A. Pan, *Adv. Mater.* **2017**, *29*, 1703256.
- [29] H. Lu, W. Tian, F. Cao, Y. Ma, B. Gu, L. Li, *Adv. Funct. Mater.* **2016**, *26*, 1296.
- [30] M. He, Y. Chen, H. Liu, J. Wang, X. Fang, Z. Liang, *Chem. Commun.* **2015**, *51*, 9659.
- [31] E. Zheng, B. Yuh, G. A. Tosado, Q. Yu, *J. Mater. Chem. C* **2017**, *5*, 3796.
- [32] M. I. Saidaminov, M. A. Haque, M. Savoie, A. L. Abdelhady, N. Cho, I. Dursun, U. Buttner, E. Alarousu, T. Wu, O. M. Bakr, *Adv. Mater.* **2016**, *28*, 8144.
- [33] M. I. Saidaminov, V. Adinolfi, R. Comin, A. L. Abdelhady, W. Peng, I. Dursun, M. Yuan, S. Hoogland, E. H. Sargent, O. M. Bakr, *Nat. Commun.* **2015**, *6*, 8724.
- [34] M. I. Saidaminov, A. L. Abdelhady, B. Murali, E. Alarousu, V. M. Burlakov, W. Peng, I. Dursun, L. Wang, Y. He, G. Maculan, A. Goriely, T. Wu, O. F. Mohammed, O. M. Bakr, *Nat. Commun.* **2015**, *6*, 7586.
- [35] G. Maculan, A. D. Sheikh, A. L. Abdelhady, M. I. Saidaminov, M. A. Haque, B. Murali, E. Alarousu, O. F. Mohammed, T. Wu, O. M. Bakr, *J. Phys. Chem. Lett.* **2015**, *6*, 3781.
- [36] T. Zhang, M. Yang, E. E. Benson, Z. Li, J. V. D. Lagemaat, J. M. Luther, Y. Yan, K. Zhu, Y. Zhao, *Chem. Commun.* **2015**, *51*, 7820.
- [37] Q. Dong, Y. Fang, Y. Shao, P. Mulligan, J. Qiu, L. Cao, J. Huang, *Science* **2015**, *347*, 967.

- [38] Z. Lian, Q. Yan, T. Gao, J. Ding, Q. Lv, C. Ning, Q. Li, J. Sun, *J. Am. Chem. Soc.* **2016**, *138*, 9409.
- [39] Y. Bi, E. M. Hutter, Y. Fang, Q. Dong, J. Huang, T. J. Savenije, *J. Phys. Chem. Lett.* **2016**, *7*, 923.
- [40] D. Shi, V. Adinolfi, R. Comin, M. Yuan, E. Alarousu, A. Buin, Y. Chen, S. Hoogland, A. Rothenberger, K. Katsiev, Y. Losovyj, X. Zhang, P. A. Dowben, O. F. Mohammed, E. H. Sargent, O. M. Bakr, *Science* **2015**, *347*, 6221.
- [41] G. Walters, B. R. Sutherland, S. Hoogland, D. Shi, R. Comin, D. P. Sellan, O. M. Bakr, E. H. Sargent, *ACS Nano* **2015**, *9*, 9340.
- [42] Y. Liu, Z. Yang, D. Cui, X. Ren, J. Sun, X. Liu, J. Zhang, Q. Wei, H. Fan, F. Yu, X. Zhang, C. Zhao, S. Liu, *Adv. Mater.* **2015**, *27*, 5176.
- [43] Y. Yang, Y. Yan, M. Yang, S. Choi, K. Zhu, J. M. Luther, M. C. Beard, *Nat. Commun.* **2015**, *6*, 7961.
- [44] Y. Dang, Y. Liu, Y. Sun, D. Yuan, X. Liu, W. Lu, G. Liu, H. Xia, X. Tao, *CrystEngComm* **2015**, *17*, 665.
- [45] L. Lee, J. Baek, K. S. Park, Y. Lee, N. K. Shrestha, M. M. Sung, *Nat. Commun.* **2017**, *8*, 15882.
- [46] B. Wenger, P. K. Nayak, X. Wen, S. V. Kesava, N. K. Noel, H. J. Snaith, *Nat. Commun.* **2017**, *8*, 590.
- [47] Z. Zuo, J. Ding, Y. Zhao, S. Du, Y. Li, X. Zhan, H. Cui, *J. Phys. Chem. Lett.* **2017**, *8*, 684.
- [48] H. Fang, S. Adjokatse, H. Wei, J. Yang, G. R. Blake, J. Huang, J. Even, M. A. Loi, *Sci. Adv.* **2016**, *2*, 1600534.
- [49] H. Diab, G. Trippe-Allard, F. Lédée, K. Jemli, C. Vilar, G. Bouchez, V. L. R Jacques, A. Tejada, J. Even, J. Lauret, E. Deleporte, D. Garrot, *J. Phys. Chem. Lett.* **2016**, *7*, 5093.
- [50] B. Wu, H. T. Nguyen, Z. Ku, G. Han, D. Giovanni, N. Mathews, H. J. Fan, T. C. Sum, *Adv. Energy Mater.* **2016**, *6*, 1600551.
- [51] J. Tilchin, D. N. Dirin, G. I. Maikov, A. Sashchiuk, M. V. Kovalenko, E. Lifshitz, *ACS Nano* **2016**, *10*, 6363.
- [52] Y. Yamada, T. Yamada, L. Q. Phuong, N. Maruyama, H. Nishimura, A. Wakamiya, Y. Murata, Y. Kanemitsu, *J. Am. Chem. Soc.* **2015**, *137*, 10456.
- [53] S. Brittan, E. C. Garnett, *J. Phys. Chem. C* **2016**, *120*, 616.
- [54] G. Grancini, V. D'Innocenzo, E. R. Dohner, N. Martino, A. R. S. Kandada, E. Mosconi, F. De Angelis, H. I. Karunadasa, E. T. Hokee, A. Petrozza, *Chem. Sci.* **2015**, *6*, 7305.
- [55] T. Baikie, N. S. Barrow, Y. Fang, P. J. Keenan, P. R. Slater, R. O. Piltz, M. Gutmann, S. G. Mhaisalkara, T. J. White, *J. Mater. Chem. A* **2015**, *3*, 9298.
- [56] Q. Han, S. Bae, P. Sun, Y. Hsieh, Y. Yang, Y. Rim, H. Zhao, Q. Chen, W. Shi, G. Li, Y. Yang, *Adv. Mater.* **2016**, *28*, 2253.
- [57] Y. Fang, Q. Dong, Y. Shao, Y. Yuan, J. Huang, *Nat. Photonics* **2015**, *9*, 679.
- [58] H. Wei, Y. Fang, P. Mulligan, W. Chuirazzi, H. Fang, C. Wang, B. R. Ecker, Y. Gao, M. A. Loi, L. Cao, J. Huang, *Nat. Photonics* **2016**, *10*, 333.
- [59] W. Wei, Y. Zhang, Q. Xu, H. Wei, Y. Fang, Q. Wang, Y. Deng, T. Li, A. Gruverman, L. Cao, J. Huang, *Nat. Photonics* **2017**, *11*, 315.
- [60] S. Yakunin, D. N. Dirin, Y. Shynkarenko, V. Morad, I. Cherniukh, O. Nazarenko, D. Kreil, T. Nauser, M. V. Kovalenko, *Nat. Photonics* **2016**, *10*, 585.
- [61] J. Zhao, G. Kong, S. Chen, Q. Li, B. Huang, Z. Liu, X. San, Y. Wang, C. Wang, Y. Zhen, H. Wend, P. Gao, J. Li, *Sci. Bulletin* **2017**, *62*, 1173.
- [62] H. S. Rao, W. G. Li, B. X. Chen, D. B. Kuang, C. Y. Su, *Adv. Mater.* **2017**, *29*, 1602639.
- [63] Y. Liu, Y. Zhang, Z. Yang, D. Yang, X. Ren, L. Pang, S. F. Liu, *Adv. Mater.* **2016**, *28*, 9204.
- [64] H. S. Rao, B. X. Chen, X. D. Wang, D. B. Kuang, C. Y. Su, *Chem. Commun.* **2017**, *53*, 5163.
- [65] Y. Chen, Q. Ge, Y. Shi, J. Liu, D. Xue, J. Ma, J. Ding, H. Yan, J. Hu, L. Wan, *J. Am. Chem. Soc.* **2016**, *138*, 16196.
- [66] M. C. Teich, B. Saleh, *Fundamentals of Photonics*, Wiley, Toronto, Canada **1991**.
- [67] J. M. Liu, *Photonic Devices*, Cambridge University Press, New York **2009**.
- [68] W. Peng, L. Wang, B. Murali, K. T. Ho, A. Bera, N. Cho, C. F. Kang, V. M. Burlakov, J. Pan, L. Sinatra, C. Ma, W. Xu, D. Shi, E. Alarousu, A. Goriely, J. He, O. F. Mohammed, T. Wu, O. M. Bakr, *Adv. Mater.* **2016**, *28*, 3383.
- [69] O. Katz, V. Garber, B. Meyler, G. Bahir, J. Salzman, *Appl. Phys. Lett.* **2001**, *79*, 1417.
- [70] J. A. Garrido, E. Monroy, I. Izpura, E. Munoz, *Semicond. Sci. Technol.* **1998**, *13*, 563.
- [71] O. Katz, G. Bahir, J. Salzman, *Appl. Phys. Lett.* **2004**, *84*, 4092.
- [72] G. Konstantatos, J. Clifford, L. Levina, E. H. Sargent, *Nat. Photonics* **2007**, *1*, 531.
- [73] F. Guo, B. Yang, Y. Yuan, Z. Xiao, Q. Dong, Y. Bi, J. Huang, *Nat. Nanotechnol.* **2012**, *7*, 798.
- [74] C. Soci, A. Zhang, B. Xiang, S. A. Dayeh, D. P. R. Aplin, J. Park, X. Y. Bao, Y. H. Lo, D. Wang, *Nano Lett.* **2007**, *7*, 1003.
- [75] Y. Yuan, J. Huang, *Acc. Chem. Res.* **2016**, *49*, 286.
- [76] K. C. Kwon, K. Hong, Q. V. Le, S. Y. Lee, J. Choi, K. B. Kim, S. Y. Kim, H. W. Jang, *Adv. Funct. Mater.* **2016**, *26*, 4213.
- [77] R. R. LaPierre, M. Robson, K. M. Azizur-Rahman, P. Kuyanov, *J. Phys. D: Appl. Phys.* **2017**, *50*, 123001.
- [78] F. Lin, L. Meng, *Int. J. Nanomanuf.* **2016**, *12*, 320.
- [79] M. A. Kats, R. Blanchard, P. Genevet, F. Capasso, *Nat. Mater.* **2013**, *12*, 20.